Journal of Ceramic Processing Research. Vol. 23, No. 2, pp. 208~212 (2022)
(Received 22 November 2021, Received in revised form 10 January 2022, Accepted 10 January 2022)
https://doi.org/10.36410/jcpr.2022.23.2.208

J O U R N A L O F
Ceramic Processing Research

Influence of synthesis parameters on phase evolution and micromorphology of lanthanum hexaaluminate

Xiaoao Li*, Jianjiang Xin, Chao Chen, Zhiqiang Du and Haotian Wang
School of Metallurgy, Northeastern University, Shenyang110819, Liaoning Province, China

Lanthanum hexaaluminate is a potential candidate for thermal barrier coatings due to its unique lamellar structure and excellent thermophysical properties. In this work, lanthanum hexaaluminate was prepared by a solid-state reaction synthesis at 1600 ºC, and the effects of aluminum source type and molding method on the phase composition and microstructure of the powder were studied. It can be seen that the synthesis efficiency of alumina as aluminium source is higher than that of aluminium hydroxide. However, the flake structure is more obvious when aluminium hydroxide is used to synthesize aluminium hydroxide. In addition, the process of compacting green compact can effectively improve the synthesis efficiency of $LaAl_{11}O_{18}$, but it will also affect the formation and growth of grains. Consequently, a high yield of $LaAl_{11}O_{18}$ powder with a particle size of 3 μm and aspect ratio of 9.88 can be obtained by compacting aluminum hydroxide as the aluminum source.

Keywords: Lanthanum hexaaluminate, Crystalline grain growth, Plate-like structure, Thermal barrier coatings.

Introduction

Hexaaluminate, as a new type of inorganic composite material, has been widely used in the nuclear industry, catalysis, electronics, superconductivity, new energy and other industries because of its special layer structure and good high-temperature performance. These materials exhibit a stable phase composition up to 1600 ºC and exceptional resistance to sintering and thermal shock, which makes them attractive materials for several applications as ceramics, matrices for immobilization of radioactive elements, catalysts for high-temperature applications, superionic conductors, and luminescent and laser materials, among others [1-5]. From the crystal structure point of view, hexaaluminate is a hexagonal layered crystal formed by alternately stacking of mirrored spinel structural units and conductive mirror surface layers along the c-axis. It belongs to the hexagonal *P*63/*mmc* spatial group and is expressed in the general formula $AAl_{11}O_{17-x}$ or $AAl_{12}O_{19-x}$. Among them, A is an alkali metal (such as Na, K, etc.), an alkaline earth metal (such as Mg, Ca, Sr, Ba, etc.), or a rare earth metal (Ln^{3+} = La, Pr, Nd, Nd, etc.), or large cations (such as Sm, Eu, Gd, etc.).

According to the ion radius, charge and number of large cations, the crystal structure of hexaaluminate is divided into β-Al_2O_3 ($AAl_{11}O_{17-x}$) and magnetite ($AAl_{12}O_{19-x}$) [4, 6]. Hexaaluminate is considered one of the most promising high-temperature materials due to its mosaicibility, excellent activity and high-temperature performance, especially in the field of thermal barrier coatings [7, 8]. Compared with the traditional Yttrium oxide partially stabilized zirconium oxide (YSZ), hexaaluminate solves the defects of YSZ such as phase transition, higher modulus and higher ablation resistance [9]. For example, $LaMgAl_{11}O_{19}$/YSZ double-layer composite thermal barrier coating formed by the introduction of Hexaaluminate exhibits better high-temperature strength and thermal shock resistance than traditional YSZ [10, 11].

Among many hexaaluminate materials, $LaAl_{11}O_{18}$ has attracted much attention due to its high melting point, low thermal conductivity and low cost. In addition to being widely used in the preparation of fluorescent materials [12] and catalysts [13], it is also used to improve the mechanical properties of alumina ceramics because of its good compatibility with Al_2O_3 [14].

Guo et al. [15] found that adding an appropriate amount of $LaAl_{11}O_{18}$ into ZIRCONIA-TOUGHENED alumina ceramics (ZTA) can improve the fracture strength and fracture toughness of ZTA ceramics through crack bridging and crack deflection effects.

Negahdari et al. [16] effectively improves the fracture toughness, hardness and elastic modulus of alumina ceramics by in-situ formation of $LaAl_{11}O_{18}$ in Al_2O_3 ceramics. In addition, more and more preparation methods are being used to further improve the performance of $LaAl_{11}O_{18}$, such as the combustion synthesis method [17, 18], coprecipitation method [19], sol-gel method [20. 21].

However, up to now, few reports have been reported on the effects of preparation methods and raw materials

*Corresponding author:
Tel : +0086-24-8368-7052
Fax: +0086-24-8368-2241
E-mail: 1710511@stu.neu.edu.cn

on the microstructures of $LaAl_{11}O_{18}$. For this purpose, $LaAl_{11}O_{18}$ was synthesized from Al_2O_3 and aluminum hydroxides using two forming processes. The effects of different aluminum sources and forming processes on the phase composition and morphology of $LaAl_{11}O_{18}$ powders were also investigated.

Experimental

Experimental procedure

In this experiment, the effects of different preparation processes (mixed powder and green body) and different aluminum sources (α-Al_2O_3 and $Al(OH)_3$) on lanthanum hexaaluminate were investigated by two preparation strategies. The flow of the first method is as follows: first, the raw materials are weighed according to the formula shown in Table 1, and then fully blended in the star ball mill. A certain amount of the blended raw material powder is then batched in a corundum crucible and placed in a muffle oven at 1600 ºC for 5 h. The second method differs from the first one by adding a molding process based on the first method, that is, the raw material is fully mixed, and then pressed into a cylindrical green billet with a diameter of 15 mm (20 MPa for 2 min), and then put into the furnace for heat treatment. To prevent the deterioration of lanthanum oxide absorbed by air from affecting the accuracy of experimental measurements, the lanthanum oxide is treated at 1100 ºC for 5 h before weighing [22].

Table 1. Formulations and forming processes of samples.

Sample code	La_2O_3	α-Al_2O_3	$Al(OH)_3$	Forming process
S-O-P	22.5	77.5	/	Mixed powder
S-OH-P	15.97	/	84.03	Mixed powder
S-O-G	22.5	77.5	/	Green body
S-OH-G	15.97	/	84.03	Green body

The starting raw materials, in this work, include α-Al_2O_3 (≥99.9%, micron-sized, Shanghai Aladdin Biochemical Technology Co., Ltd., Shanghai, China), $Al(OH)_3$ (analytical-grade purity, Sinopharm Chemical Reagent Co., Ltd, Shanghai, China), and La_2O_3 (analytical-grade purity, Sinopharm Chemical Reagent Co., Ltd, Shanghai, China).

Characterization

X-ray powder diffraction (XRD, Bruker D8-Advance, Germany) was used to characterize the phase composition of powder samples, with a scan speed of 4 °·min^{-1} (2θ = 15° – 85°). A scanning electron microscope (SEM, Hitachi S-4800, Japan) was applied to record the micromorphology of the samples, and energy dispersive spectroscopy (EDS) was used to qualitatively analyze the micro-constitution of the samples. In addition, the relative amounts of $LaAlO_3$ in different samples were calculated by equation (1) [23].

$$M_{LaAlO_3} = \frac{I_{LaAlO_3}}{I_{LaAlO_3} + 0.5 \times (I_{107} + I_{114})} \times 100\% \quad (1)$$

Where M_{LaAlO3} is the relative amount of $LaAlO_3$; I_x is the intensity of a given peak of $LaAlO_3$ or $LaAl_{11}O_{18}$.

Results and Discussion

Fig. 1 shows the XRD patterns of different samples after being calcined at 1600 ºC for 5 h, and their main crystalline phases are $LaAl_{11}O_{18}$, and their secondary crystalline phases are $LaAlO_3$ and α-Al_2O_3. Compared with different aluminum source samples (such as samples S-O-P or S-OH-P), the relative intensity of the diffraction peak of $LaAl_{11}O_{18}$ in the XRD spectrum of sample S-O-P synthesized from alumina is higher, which means that the target phase content is higher, as

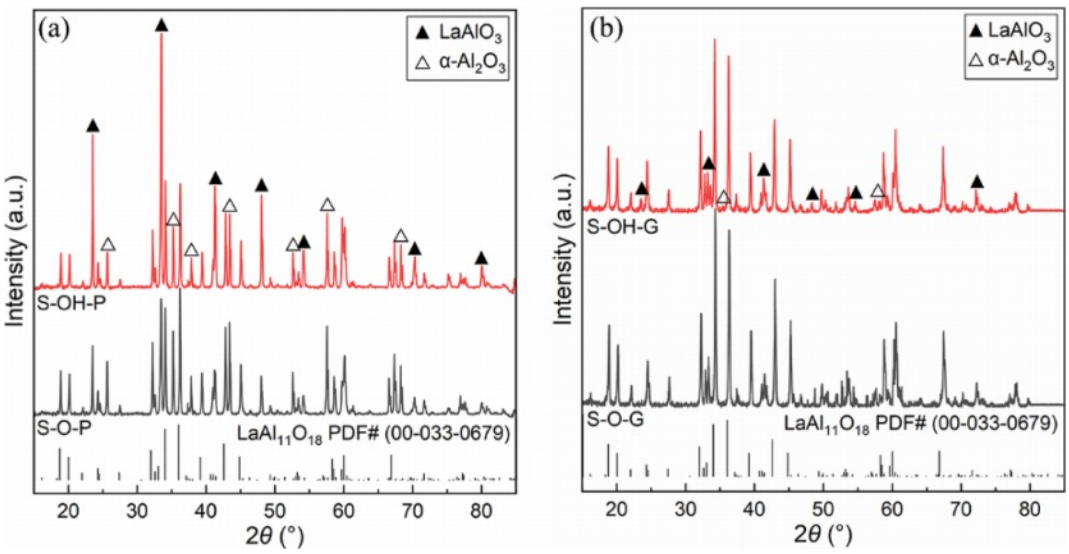

Fig. 1. XRD patterns of different samples.

shown in Fig. 1(a). Compared with different forming process samples (such as samples S-O-P or S-O-G), the XRD spectra of sample S-O-G synthesized from green samples have a lower relative intensity of the diffraction peaks of the intermediate products ($LaAlO_3$ and α-Al_2O_3), which means that the reaction is more complete as shown in Fig. 1(b).

From the reaction mechanism, alumina first reacts with lanthanum oxide and form $LaAlO_3$, then continues to react with $LaAlO_3$ and form $LaAl_{11}O_{18}$ [24]. In addition, existing studies have shown that the direct use of $MgAl_2O_4$ as raw material for the synthesis of $LaMgAl_{11}O_{19}$ has a higher synthesis efficiency than that of MgO [25]. Therefore, samples synthesized from green compacts have shorter distances to achieve solid-state reactions at high temperatures by atom diffusion and require lower activation energy, so the synthesis efficiency is higher. In addition, although the decomposition of $Al(OH)_3$ results in high activity γ-Al_2O_3, however, because it can only participate in the formation of $LaAlO_3$ (γ-Al_2O_3 is converted to α-Al_2O_3), so it does not affect the reaction between $LaAlO_3$ and $LaAl_{11}O_{18}$. In addition, to quantify the synthesizing effect of different samples, the content of $LaAlO_3$ in different samples was further calculated, as shown in Fig. 2. By comparing the experimental results, it can be seen that the content of $LaAlO_3$ in molded sample with alumina as aluminum source is the least and the synthesis efficiency is the highest.

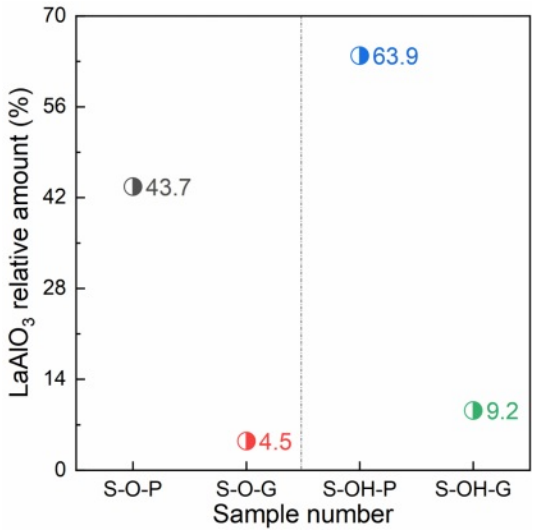

Fig. 2. Relative amount of $LaAlO_3$ in different samples.

Fig. 3 presents the SEM images of different samples

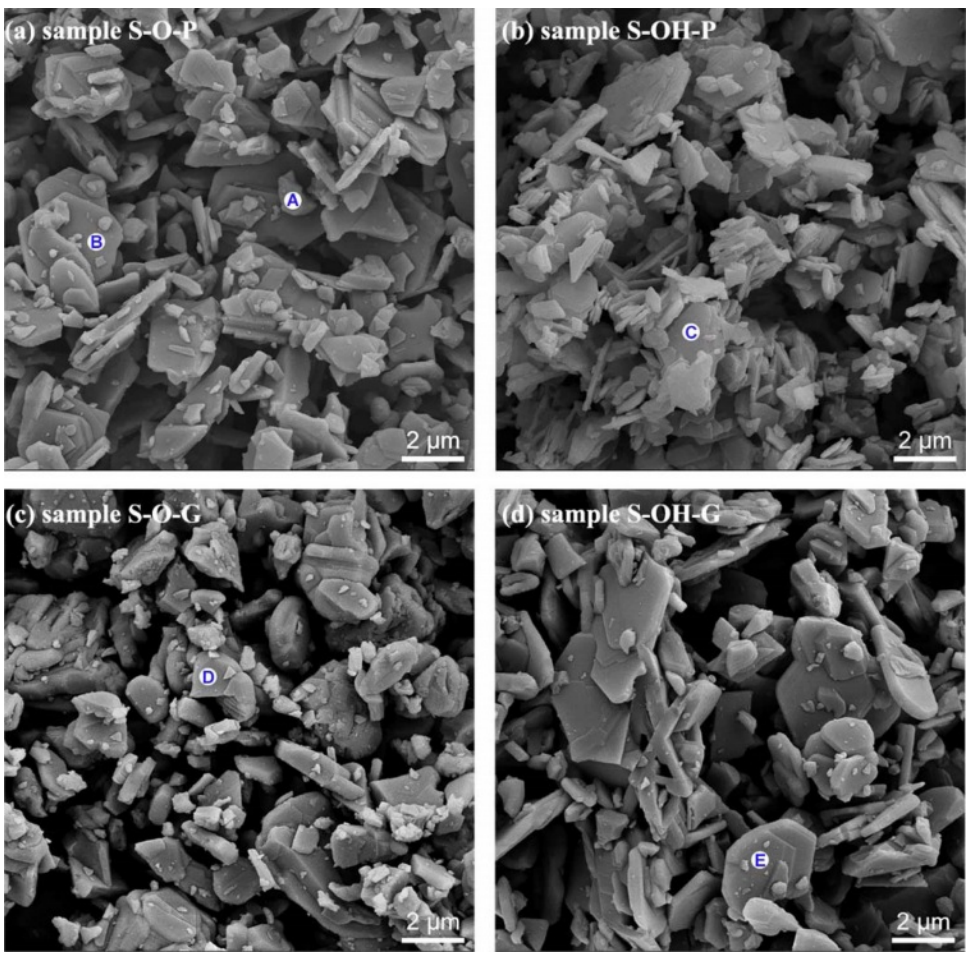

Fig. 3. SEM images of the different samples.

Table 2. EDS results of different samples shown in Fig. 3 (at.%).

Points	La	Al	O	Possible phase
A	18.93	19.52	61.55	$LaAlO_3$
B	2.73	37.85	59.42	$LaAl_{11}O_{18}$
C	3.18	37.29	59.53	$LaAl_{11}O_{18}$
D	3.66	36.31	60.03	$LaAl_{11}O_{18}$
E	4.56	36.46	58.98	$LaAl_{11}O_{18}$

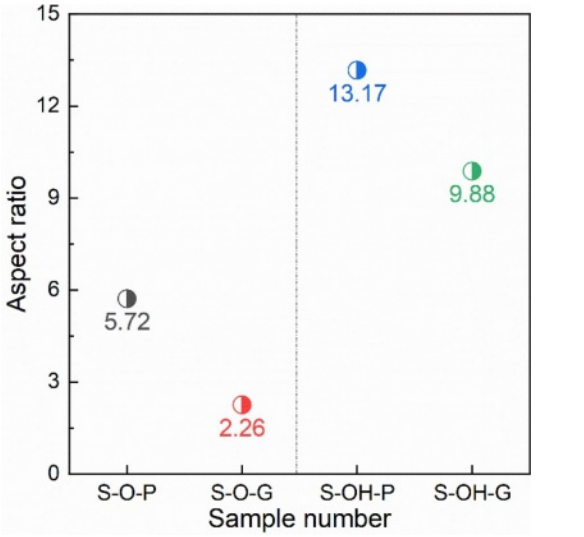

Fig. 4. Aspect ratios of the different samples.

after being calcined at 1600 °C for 5 h. For samples S-O-P and S-O-G, their grains show two micron-scale structures, plate-like and granular, and sample S-O-G has no obvious flaking of sample S-O-P (Fig. 3(a) and (c)). Combining the EDS results shown in Table 2 with corresponding XRD patterns, it can be seen that the lamellar grains of sample S-O-P are $LaAl_{11}O_{18}$, and the granular grains are $LaAlO_3$, which is an unresponsive intermediate phase. The granular grains of sample S-O-G are still $LaAl_{11}O_{18}$. Similarly, comparing the SEM images of samples S-OH-P and S-OH-G, it is found that the grain size of sample S-OH-P synthesized directly from powders is smaller (~1 μm), the plate grain thickness is relatively thin. The grain development of sample S-OH-P synthesized from compacted billet is higher (~3 μm). In addition, the EDS results of points C and E indicate that all lamellar grains are $LaAl_{11}O_{18}$, as shown in Table 2.

Combined with the growth mechanism of $LaAl_{11}O_{18}$ crystal, there are two reasons why the samples exhibit different microstructures. Firstly, as mentioned earlier, the crystallization behavior of $LaAl_{11}O_{18}$ with plate structure is determined by its own crystal structure. $LaAl_{11}O_{18}$ belongs to the structure of magnetite lead ore and is characterized by a layer of lanthanum oxide and an aluminum spinel (γ-Al_2O_3) sandwiched between the layers of lanthanum oxide (La_2O_3). La_2O_3 layer is a crystallographic mirror structure, with γ-Al_2O_3 layer symmetrically mirrored on both sides. In the La_2O_3 layer, O^{2-} is closely packed in a hexagonal shape, and La^{3+} is in a compact stacked structure of O^{2-}. In such a structure, $LaAl_{11}O_{18}$ is more likely to grow perpendicular to the c-axis because the diffusion of oxygen ions is inhibited, while growth along the c-axis is inhibited [26]. Secondly, the lamellar structure of sample S-OH-G synthesized from $Al(OH)_3$ as the aluminum source is more evident, which may be due to the free growth of $LaAl_{11}O_{18}$ along the c-axis due to the space required for the grain orientation growth of $LaAl_{11}O_{18}$ left by the decomposition of $Al(OH)_3$ at high temperature [27, 28]. Similarly, when α-Al_2O_3 is used as the aluminum source, the plate shape of sample S-O-P synthesized directly from the powder is more obvious than that of sample S-O-G synthesized from the pressed green compact.

Furthermore, Fig. 4 shows the aspect ratios of different samples calculated by statistics. The aspect ratio of $LaAl_{11}O_{18}$ powders synthesized with $Al(OH)_3$ as the aluminum source is larger. Considering the degree of crystallization, sample S-OH-G synthesized from compacted raw billet with $Al(OH)_3$ as the source of aluminum is the best choice for obtaining good micromorphology.

Conclusions

In this work, $LaAl_{11}O_{18}$ powders were synthesized by solid-state reaction at 1600 °C for 5 h, and the influence of aluminum source and forming process on the phase composition and micro-morphology of the prepared $LaAl_{11}O_{18}$ powders was investigated. Based on the above results and analysis, the following conclusions can be drawn.

From the synthesizing efficiency, alumina is more efficient as the aluminum source than aluminum hydroxide, and the compacted billet is more efficient than the powder. Specifically, using alumina as the aluminum source, the content of the $LaAlO_3$ intermediate phase in the synthetic powder can be reduced from 63.9% (sample S-OH-P) to 43.7% (sample S-O-P). The content of the $LaAlO_3$ intermediate phase in synthetic powder can be further reduced from 43.7% to 4.5% (sample S-O-G) by green compaction.

From the grain morphology, it is more obvious to use aluminum hydroxide as the aluminum source for the flaking, and the compaction of the raw billet can inhibit the grain orientation growth. Generally speaking, aluminum hydroxide plus green compaction is the best choice. The grains of $LaAl_{11}O_{18}$ powder synthesized are fully lamellar with an aspect ratio of 9.88.

Declarations

Conflicts of interests The authors declare that they have no competing interests.

References

1. N. Nayebpashaeea, S.H. Seyedeina, M.R. Aboutalebia, H. Sarpoolakyb, and M.M. Hadavic, J. Ceram. Process. Res. 17[8] (2016) 803-814.
2. J.J. Torrez-Herrera, S.A. Korili and A. Gil, Catal. Rev. (2020) 1-39.
3. M.A. Khan, M. Duraiselvam, S.S. Panwar, T. Jena, and S.R. Dhineshkumar, Surf. Coat. Technol. 321[15] (2017) 146-155.
4. M. Tian, X.D. Wang, and T. Zhang, Catal. Sci. Technol. 6[7] (2016) 1984-2004.
5. J.S. Li and Y.L. Liu, Trans. Trans. Indian Ceram. Soc. 73[4] (2014) 270-276.
6. D. Holtstam and U. Hålenius, Mineral. Mag. 84[3] (2020) 376-380.
7. R. Vaßen, M.O. Jarligo, T. Steinke, D.E. Mack, and D. Stöver, Surf. Coat. Technol. 205[4] (2010) 938-942.
8. D. Lee, C. Kim, K. Lee, and B. Jang, J. Ceram. Process. Res. 20[5] (2019) 499-504.
9. H. Jamali, R. Mozafarinia, R.R. Shoja, and P.R. Ahmadi, Ceram. Int. 38[8] (2012) 6705-6712.
10. X.L. Chen, Y. Zhao, X.Z. Fan, Y.J. Liu, B.L. Zou, Y. Wang, H.M. Ma, and X.Q. Cao, Surf. Coat. Technol. 205[10] (2011) 3293-3300.
11. J.W. Lee, C.H. Lee, and H.J. Kim, J. Ceram. Process. Res. 2[3] (2001) 113-119.
12. V. Singh, G. Sivaramaiah, J.L. Rao, S.J. Dhoble, and S.H. Kim, Mater. Chem. Phys. 149 (2015) 202-208.
13. H.M. Ai, H.Y. Yang, Q. Liu, G.M. Zhao, J. Yang, and F.N. Gu, Chin. J. Catal. 39[2] (2018) 297-308.
14. E.T. Fritsche and L.G. Tensmeyer, J. Am. Ceram. Soc. 50[3] (1967) 167-168.
15. R. Guo, D. Guo, Y. Chen, Z. Yang, and Q. Yuan, Ceram. Int. 28[7] (2002) 699-704.
16. Z. Negahdari, M. Willert-Porada, and C. Pfeiffer, Mater. Sci. Eng. A 527[12] (2010) 3005-3009.
17. V. Singh, N. Singh, M.S. Pathak, S. Watanabe, T.K.G. Rao, P.K. Singh, and V. Dubey, Optik 157 (2018) 1391-1396.
18. J. Baseri, R. Naghizadeh, and H.R. Rezaie, J. Ceram. Process. Res. 18[1] (2017) 21-26.
19. Y.Q. Wu, Y.F. Zhang, X.X. Huang, B. Li , and J.K. Guo, J. Mater. Sci. 36[17] (2001) 4195-4199.
20. P. Jana, P.S. Jayan, S. Mandal, and K. Biswas, J. Cryst. Growth. 408 (2014) 7-13.
21. B.K. Park, Y.S. Lee, and K.K. Koo, J. Ceram. Process. Res. 11[1] (2010) 64-68.
22. X.K. Li, X.J. Mao, M.H. Feng, S. Qi, B.X. Jiang, and L. Zhang, J. Eur. Ceram. Soc. 36[10] (2016) 2549-2553.
23. J.B. Sun, J.S. Wang, W.Z. Huang, Y. Hui, X. Zhou, L.F. Li, J.N. Jiang, L.H. Deng, Y.Y. Niu, S.J. Dong, and X.Q. Cao, J. Rare Earths. 35[12] (2017) 1226-1232.
24. R.C. Ropp and B. Carroll, J. Am. Ceram. Soc. 63[7] (1980) 416-419.
25. M.M. Khorramirad, M.R Rahimipour, S.M.M. Hadavi, and K.S. Jozdani, Ceram. Int. 44[5] (2018) 4734-4739.
26. P.L. Chen and I.W. Chen, J. Am. Ceram. Soc. 75[9] (1992) 2610-2612.
27. H. Song and R.L. Coble, J. Am. Ceram. Soc. 73[7] (1990) 2077-2085.
28. H. Song and R.L. Coble, J. Am. Ceram. Soc. 73[7] (1990) 2086-2090.